Cavitation Nuclei Population and Event Rates

Zhenhuan Liu
Graduate Student.

Christopher E. Brennen
Professor.

Division of Engineering
and Applied Science,
California Institute of Technology,
Pasadena, CA 91125

To model the processes of cavitation inception, noise and damage, it is necessary to generate a model of the cavitation event rate which can then be coupled with the consequences of the individual events to produce a complete synthesis of the phenomenon. In this paper we describe recent efforts to connect the observed event rates to the measured distributions of cavitation nuclei in the oncoming stream. Comparisons are made between the observed event rates and event rates calculated from measured nuclei distributions using an algorithm which includes the dynamics of the nuclei motion and growth. Various complications are explored including the effect of the boundary layer, the relative motion between the nucleus and the liquid, the observable bubble size effect, and the effect of bubble growth on neighboring nuclei. All of these are seen to have important influences on the event rate, and therefore, on cavitation inception and other macroscopic consequences. We demonstrate that it is possible to predict the correct order of magnitude of the event rate when an attempt is made to model the important flow complications.

1 Introduction

In order to synthesize the cumulative effects of a stream of traveling cavitation bubbles, it is necessary to supplement the details of individual events with the rates at which these events occur. Many investigators have anticipated a relationship between the cavitation event rate and the concentration of cavitation nuclei in the oncoming stream (see, for example, Schiebe, 1972; Keller, 1972, 1974; Keller and Weitendorf, 1976; Kuiper, 1978; Gates and Acosta, 1978; Meyer et al., 1992). At first sight this seems like a straightforward problem of computing the flux of nuclei into the region for which $C_p < -\sigma$. However, many complications arise which make this analysis more difficult than might otherwise appear and we shall discuss some of the specific issues below. But these difficulties do not account for the lack of experimental research into the relationship. Rather, the difficulties involved in the accurate measurement of the incoming nuclei number distribution function, $N(R)$, have been responsible for the delay in any detailed, quantitative investigation of this component of the problem. (Note that $N(R)dR$ is the number of nuclei with size between R and $R + dR$ per unit volume.) As Billet (1985) remarked in his review of nuclei measurement techniques, the only reliable method of obtaining $N(R)$ has been the extremely time-consuming procedure of surveying a reconstruction of an in situ hologram of a small volume of tunnel water (Gates and Bacon, 1978). However, the time and effort required to construct one $N(R)$ distribution by this method has seriously limited the scope of these investigations.

The recent development of light scattering instruments employing phase Doppler techniques (Saffman et al., 1984; Tanger et al., 1992) has improved the situation. In our laboratory, we have succeeded in validating and calibrating a Phase Doppler Anemometer (PDA) made by Dantec by taking simultaneous measurements with the PDA and a holographic system (Liu et al., 1993). The great advantage of the PDA system is the speed with which $N(R)$ can be measured. After validation, the PDA system could then be used with confidence for investigations of the nuclei population dynamics in a water tunnel (Liu et al., 1993 and 1994) and of the aforementioned relation between $N(R)$ and the cavitation event rate (Liu et al., 1993, Liu and Brennen, 1994).

In this paper, we first present the experimental observations of cavitation event rates on a Schiebe headform with simultaneous measurement of the nuclei distribution in the upcoming stream. We then present an analytical model to synthesize the event rates from the measured nuclei distributions. Then we compare the predicted event rates with cavitation observations in two water tunnels with quite different nuclei population dynamics.

2 Observations of Nuclei Population and Event Rates

The experiments were performed in the Low Turbulence Water Tunnel (LTWT) and the High Speed Water Tunnel (HSWT) at Caltech. Detailed descriptions of these two water tunnels can be found in other literature (see Gates, 1978 and Liu and Brennen, 1995), and will not be repeated here. Figure 1 shows a sketch of the experimental setup. A Schiebe headform with 5.08 cm diameter was installed at the center of the water tunnel. The free-stream nuclei number distribution was measured by a Phase Doppler Anemometer (PDA), which was calibrated by comparing the results with those obtained by a holographic method (Liu et al., 1993). On the other hand, the cavitation event rate on the Schiebe headform was measured by three flush-mounted electrodes on the headform surface (Ceccio and Brennen, 1992 and Kuhn de Chizelle et al., 1992).

In Fig. 2, we present a typical comparison of the nuclei number density distributions in the LTWT and in the HSWT. Also plotted in the figure are measurements in other facilities (Arndt and Keller, 1976; Peterson et al., 1972, 1975; Feldberg and Shlemenson, 1971; Keller and Weitendorf, 1976; and Gates and Bacon, 1978) and in the ocean (Cartmill and Su, 1993). As expected, substantial differences in the nuclei number density distributions in the two water tunnels were found. Although the shapes of the distributions are similar, the differences in the magnitudes were as much as two orders of magnitude. The typical nuclei concentration in the LTWT is quite large, about 100 cm^{-3}; while the nuclei concentration in the HSWT is low at about 1 cm^{-3}. Billet (1985) and Gindroz and Billet (1994) presented useful reviews of the subject of nuclei concentrations and distributions. They found that for deaerated water, typical concentrations are of the order of 20 cm^{-3} with sizes ranging from about 5 μm to about 20 μm. We conclude that the LTWT is nuclei rich and the HSWT is nuclei poor. This was expected

Contributed by the Fluids Engineering Division for publication in the JOURNAL OF FLUIDS ENGINEERING. Manuscript received by the Fluids Engineering Division August 8, 1995; revised manuscript received October 2, 1997. Associate Technical Editor: J. Katz.

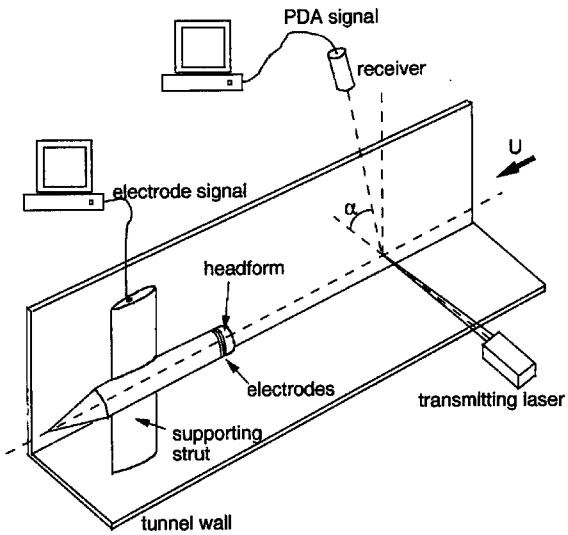

Fig. 1 Experimental setup for the simultaneous measurement of the cavitation nuclei distribution in the water tunnel and the cavitation event rate on a Schiebe headform

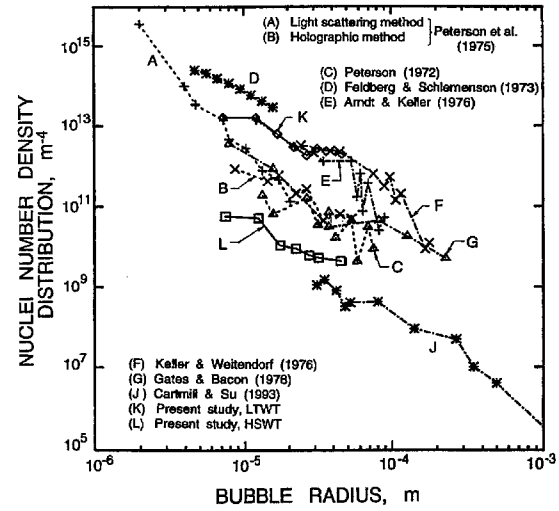

Fig. 2 A comparison of the nuclei number density distributions in the Low Turbulence Water Tunnel and the High Speed Water Tunnel with measurements in other facilities and in the ocean. The uncertainty in the ordinate is ±5 percent.

since the HSWT has an effective resorber while the LTWT does not; related studies (Liu, 1995, Liu et al., 1993) demonstrated that, as a result, the two facilities have quite different nuclei population dynamics. Consequently, comparative experiments in the two tunnels were expected to provide a valuable range of nuclei populations.

Figure 3 presents the measurements of the event rates on a Schiebe headform in the LTWT and HSWT tunnels. Note that the cavitation event rates increase dramatically as the cavitation number is decreased. However, the event rates can vary by as much as a decade at the same cavitation number. At the same cavitation number, the larger free stream nuclei concentrations correspond to the larger cavitation event rates. As one would expect, the event rates observed at the same cavitation number in the LTWT are much higher than in the HSWT, because of the much higher nuclei population in the LTWT.

During the tests in the HSWT, cavitation experiments were performed at various speeds and air contents. Again, it was clear that the nuclei population had a strong effect on the cavitation event rate as illustrated on the right in Fig. 3. This resulted in a significant effect on the cavitation inception number. For example, at a velocity of 9.4 m/s and a nuclei concentration of 0.8 cm^{-3}, the cavitation inception number was 0.47. After air injection, the nuclei concentration rose to 12 cm^{-3}, and cavitation inception occurred at $\sigma_i = 0.52$. In contrast, in the LTWT, the cavitation inception number in the LTWT was about 0.57, and the nuclei concentration was about 100 cm^{-3}. In the HSWT, attached cavitation occurred soon after traveling bubble cavitation. This implies that attached cavitation occurs more readily when the nuclei population is low. Similar phenomenon was also observed by Li and Ceccio (1994) on a cavitating hydrofoil. In their observations, when the nuclei concentration in the

Nomenclature

C = nuclei concentration
C_P = coefficient of pressure, $(p - p_\infty)/\frac{1}{2}\rho U^2$
C_{PM} = minimum C_P on a given streamline
C_{PMS} = minimum value of C_P on the headform surface
C^*_{P1} = constant
D = headform diameter
E = cavitation event rate
$N(R)$ = nuclei density distribution function
R = radius of a cavitation nucleus
$\dot{R}, \ddot{R} = dR/dt, d^2R/dt^2$
R_C = critical cavitation nucleus radius
R_M = minimum observable bubble radius
R_{max} = maximum cavitation bubble radius
R_0 = initial nucleus radius
S = surface tension
U = upstream tunnel velocity
U_M = maximum velocity corresponding to C_{PMS}
f_1, f_2, f_3 = numerical factors effecting the cavitation event rate
n_i = bubble/bubble interaction effect
p = fluid pressure
p_∞ = free stream pressure
p_{G0} = initial gas pressure in a bubble
p_c = blake critical pressure
p_{min} = undisturbed liquid pressure
p_v = vapor pressure
q = flow velocity
r = distance from the center of a bubble
r_H = headform radius
r_K = radius of curvature of streamlines near minimum pressure point
r_S = radius of minimum pressure point
r_e = critical radius
y = distance normal to body surface
y_M = maximum y value of the $C_P = -\sigma$ isobar
s, s_0 = coordinate along a streamline and the location of minimum pressure point
t_G = time available for bubble growth
u, u_M = fluid velocity, fluid velocity just outside boundary layer
v = velocity of a bubble normal to streamline
ρ = fluid density
σ = cavitation number, $(p_v - p_\infty)/\frac{1}{2}\rho U^2$
σ_{cri} = threshold cavitation number
σ_i = inception cavitation number
σ'_i = cavitation number variation
ξ, λ = factors in the chosen analytical expression for $N(R)$
ν = kinematic viscosity of fluid
μ = fluid viscosity
δ, δ_2 = thickness and momentum thickness of the boundary layer
ϵ = displacement of a bubble normal to a streamline
Σ = function defined by Eq. (15)
$\Sigma' = d\Sigma/d(r/r_H)$

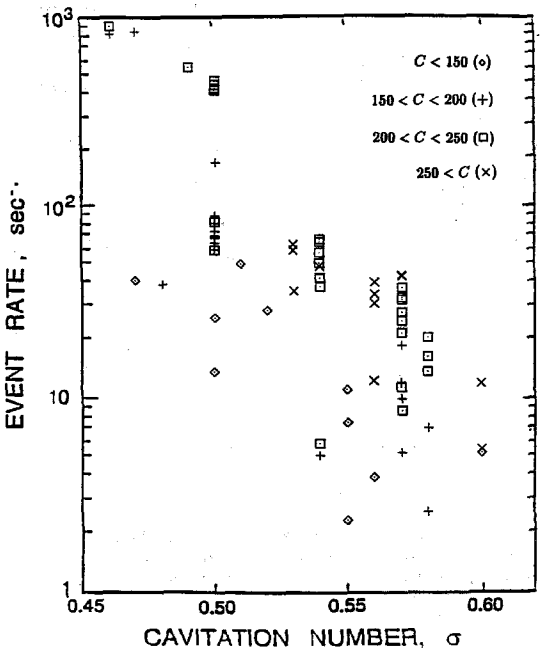

Fig. 3 Left: Variations in the cavitation event rates with cavitation number on a 5.08 cm Schiebe body in the LTWT at a speed of 9 m/s. Data are plotted for various ranges of free stream nuclei concentration, C (cm^{-3}): $C < 150$ (◇); $150 < C < 200$ (+); $200 < C < 250$ (□) and $250 < C$ (×).

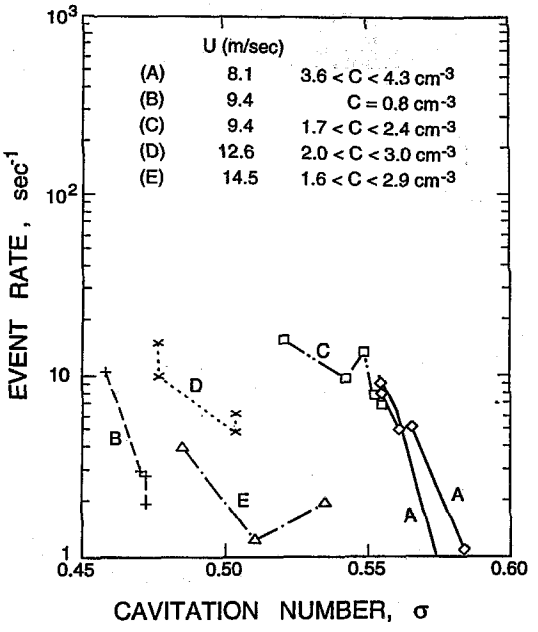

Fig. 3 Right: Observed cavitation event rates on a 5.08 cm Schiebe body in the HSWT at various tunnel speeds and nuclei concentrations. The data are plotted for various tunnel speeds and nuclei concentrations. The uncertainty in the ordinate is ±5 percent.

water was high, traveling bubble cavitation occurred before attached cavitation was observed. But when the nuclei concentration was low, no traveling bubble cavitation was observed before attached cavitation occurred. They ascribe the cause of this phenomenon to laminar boundary separation on the hydrofoil. However, we are not sure about the cause on the Schiebe headform since it does not exhibit laminar boundary layer separation in the region of low pressure where these events were observed.

By comparing the event rates for conditions C and E in Fig. 3 (right), it can be seen that, at the constant nuclei concentration level, the cavitation event rate decreased with increasing tunnel velocity, which is the inverse of what would be expected. All the numerical and analytical simulations (Ceccio and Brennen, 1992; Meyer et al., 1992; Liu et al., 1993) predict that the event rate increases with oncoming velocity, provided that the nuclei population remains the same. This velocity effect on the cavitation event rate was also observed by Kuhn de Chizelle et al. (1992, 1995). Since they were unable to measure the nuclei population in the oncoming flow, Kuhn de Chizelle et al. speculated that the free nuclei population was decreased by the increase in tunnel pressure necessary to achieve the same cavitation number at a higher speed. The investigations of nuclei population dynamics in a water tunnel by Liu et al. (1993) support that explanation. However, the current data shows that the event rates decrease with an increasing tunnel speed even when the nuclei concentrations are at the same level. This phenomenon is not understood. A possible explanation is that the PDA mistakenly counted more solid particles as microbubbles at the higher tunnel velocities. Since the population of solid particles increased with speed, perhaps the number of microbubbles decreased even though the total nuclei concentration remained the same. It may also be the case that there exists some, as yet unrecognized, mechanism in the relation between the nuclei population and the cavitation event rate.

3 An Analytical Model for Cavitation Event Rate

A simple synthesis of the cavitation event rate from the nuclei distribution in the on-coming stream was presented by Ceccio and Brennen (1992). Here we explore this relationship further and comment on other factors which could significantly effect the event rate. We will use a nuclei number distribution function, $N(R)$, defined such that, per unit volume, the number of nuclei with radii between R and $R + dR$ is given by $N(R)dR$. From the measurement of free stream nuclei distribution in our laboratory (see Liu et al., 1993), a characteristic form for $N(R)$ is

$$N(R) = C\frac{\log e}{(2\pi)^{1/2}\lambda R}\exp\left(-\frac{(\log R - \log \xi)^2}{2\lambda^2}\right) \quad (1)$$

where C is the nuclei concentration. By adjusting the values of ξ and λ, the distribution function (1) can be made to fit most observed nuclei distribution functions. It is preferable to the more frequently used power law because it allows simulation of the peak in the population which is often observed (at $R = \xi$) and of the fact that the population of large bubbles is very small.

The principal problem in synthesizing the event rate is to evaluate how many of these nuclei are convected into the region of low pressure near the minimum pressure point on the surface of the body and how many therefore grow to observable macroscopic vapor bubbles. Some simplifying observations allow us to avoid lengthy numerical computations of the bubble dynamics (using the Rayleigh-Plesset equation) for every nucleus size, every streamline, every cavitation number, etc. Meyer et al. (1989, 1992) conducted a detailed numerical study of this kind which included most of the effects studied here. In this paper we present a much simpler analytical approach which, though more approximate, is probably as accurate as the current experimental data would merit. First, we shall employ various relations pertaining to spherical bubble dynamics despite the tact that, as shown by Ceccio and Brennen (1992), the actual cavitation bubbles are far from spherical. However, Kuhn de Chizelle et al. (1995) also showed that the Rayleigh-Plesset equation gives a reasonable though crude estimate of the bubble dimensions and we therefore adopt this approximation here. However, in doing so we note that Kuhn de Chizelle et al. (1995) also demonstrated increasing departure from sphericity and from the

Rayleigh-Plesset equation for the larger bubbles at low cavitation numbers and we make reference to this in discussing the results.

Ceccio and Brennen (1992) observed while carrying out numerical integration of the Rayleigh-Plesset equation that, for a given cavitation number, σ, and minimum pressure coefficient, C_{PM}, all nuclei above a certain critical size, $R = R_C$, would grow to roughly the same observable bubble size and therefore would be registered as "cavitation events." Furthermore, the critical size, R_C, appeared to be almost independent of the details of the pressure/time history and a function only of the difference between the minimum pressure and the vapor pressure (represented non-dimensionally by $(-C_{PM} - \sigma)$), the upstream velocity, U, the fluid density, ρ, and surface tension, S. Specifically,

$$R_C = \frac{8\beta S}{3\rho U^2(-C_{PM} - \sigma)} \tag{2}$$

fitted the bubble dynamic calculations very well when the empirical parameter $\beta \approx 1$. This expression is, of course, consistent with the stability analyses put forward first by Flynn (1964) and Johnson and Hsieh (1966). Its use does save a great deal of computational effort. Furthermore, it means that we need not concern ourselves with the detailed pressure/time history along the entire length of each streamline but can simply focus on the region around the minimum pressure point.

However, it is necessary to determine how the minimum pressure coefficient, C_{PM}, varies from streamline to streamline. Here again we will use a simple analytic expression derived from much more complex computations. A panel method was developed to solve the potential flow around any axisymmetric headform. This was used to calculate the potential flow around the Schiebe headform. Such calculations suggested that the pressure gradient, dp/dy, normal to the surface in the vicinity of the minimum pressure point could be approximated by $\rho U_M^2/r_K$ where $U_M = U(1 - C_{PMS})^{1/2}$ and C_{PMS} are, respectively, the velocity and pressure coefficient at the minimum pressure point on the surface of the body (exterior to the boundary layer) and r_K is a measure of the radius of curvature of the streamlines in this region. For the Schiebe body ($C_{PMS} = -0.78$) it is found that $r_H/r_K = 2.5$ provides an approximate representation of the variation in the minimum pressure coefficient, C_{PM}, on a streamline with the distance y of that streamline from the surface. The actual variation of C_{PM} with y from the potential flow calculation is shown in Fig. 4 along with several approximations. With $dp/dy = \rho U_M^2/r_K$ it follows that

$$C_{PM} = C_{PMS} + 2y(1 - C_{PMS})/r_K \tag{3}$$

This expression allows us to evaluate from Eq. (2) the critical nuclei size, $R_C(y)$, for each streamline. Clearly, R_C increases with the distance, y, of the streamline from the surface. A larger critical size means that fewer of the available nuclei will generate cavitation events. The process is terminated on that streamline which just touches the isobar $C_{PM} = -\sigma$ for then the minimum pressure is equal to the vapor pressure and no cavitation events will occur on this streamline or any outside it. Consequently, we need only be concerned with a region near the surface given by

$$0 < y \leq y_M f_3 \tag{4}$$

where

$$y_M = \frac{(-C_{PMS} - \sigma)}{2(1 - C_{PMS})} r_K \tag{5}$$

and $f_3 = 1$. Different values of f_3 which is a function of R_M/r_H will be used later to examine the influence of a minimum observable bubble size, R_M. Using the relations (2) and (3) and disregarding any possible effects of the boundary layer or of relative motion between the nucleus and the flow one can then construct an event rate from the nuclei number distribution as follows. The volume flow rate passing through two stream surfaces a distance, dy, apart at the minimum pressure point (see Fig. 5) is given by

$$2\pi r_S U(1 - C_{PMS})^{1/2} f_1(y) dy \tag{6}$$

where $f_1(y) = 1$, but different values will be used later to account for the same boundary layer effects. The variable r_S is the radial distance from the axis of symmetry to the minimum pressure point (on the Schiebe body $r_S/r_H \approx 0.75$). It follows from Eq. (6) that the cavitation event rate in the stream tube, dE, is given by

$$dE = 2\pi r_S U(1 - C_{PMS})^{1/2} f_1(y) dy \times \int_{R_C(y)}^{\infty} \frac{N(R)dR}{f_2(R, y)(1 + n_i)} \tag{7}$$

where $f_2(R, y) = 1$, but different values will be used later to account for screening effects due to relative motion between the nuclei and the liquid. Also $n_i = 0$, but different values will be used later to account for the bubble/bubble interactions. In the above equation it follows from Eqs. (2) and (3) that

$$R_C(y) = \frac{8\beta S}{3\rho U^2}\left[-\sigma - C_{PMS} - \frac{2y(1 - C_{PMS})}{r_K}\right]^{-1} \tag{8}$$

Note that $R_C(y \to y_M) \to \infty$. It follows that the total cavitation event rate, E, will be

$$E = \int_0^{y_M f_3} 2\pi r_S U(1 - C_{PMS})^{1/2} f_1(y) \times \int_{R_C(y)}^{\infty} \frac{N(R)dR}{f_2(R, y)(1 + n_i)} dy \tag{9}$$

where $f_3 = 1$, but different values will be used to account for the observable bubble size effect.

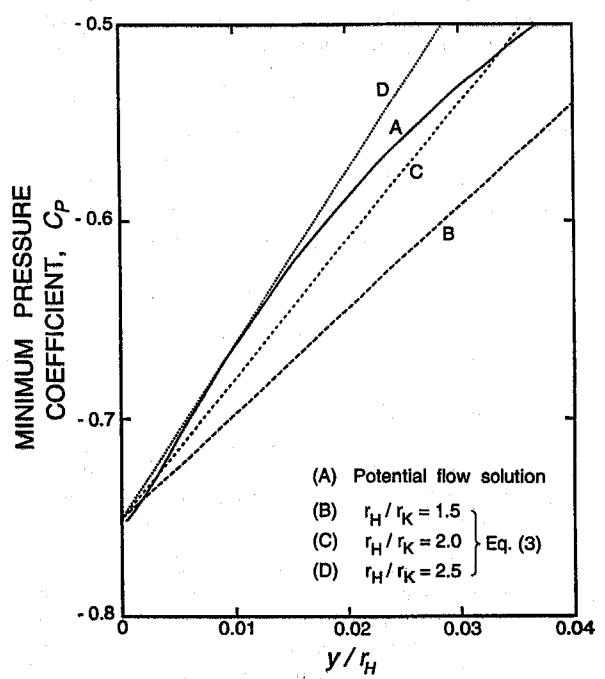

Fig. 4 Variation in the minimum pressure coefficient, C_{PM}, on a streamline for a Schiebe headform with the distance y of that streamline from the surface of the body near the minimum pressure point

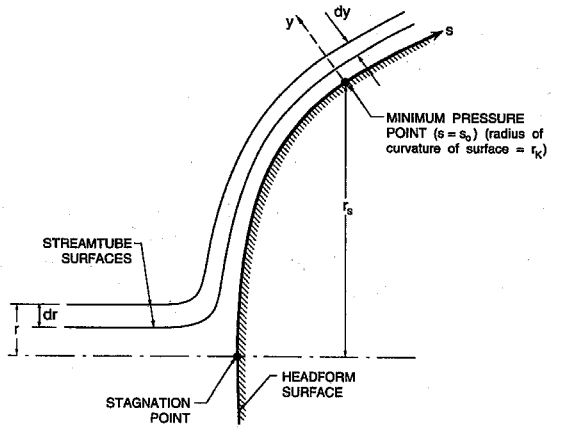

Fig. 5 Schematic showing a typical annular stream tube upstream of the headform and in the neighborhood of the minimum pressure point

3.1 Boundary Layer Effect. The above analysis neglected the effects which the presence of a boundary layer might have on the pressure/time history experienced by a potential cavitation nucleus. Several such effects can be envisaged. These include the fact that the boundary layer will reduce the volume flow rate of fluid traveling close to the headform and thus reduce the supply of nuclei. It will also increase the residence time of the bubbles in a thin layer very close to the surface, though estimates of this effect indicate that it is not a major factor. It may also alter the shape of the isobars near the surface. Here we will explore only the first of these effects. To do so we assume a simple form for the boundary layer profile near the minimum pressure point, namely,

$$\frac{u}{U_M} = \begin{cases} 2\left(\frac{y}{\delta}\right) - 2\left(\frac{y}{\delta}\right)^3 + \left(\frac{y}{\delta}\right)^4 & \text{for } y < \delta \\ 1 & \text{for } y \geq \delta \end{cases} \tag{10}$$

where δ is the boundary layer thickness. If δ_2 is the momentum thickness, it follows that $\delta_2 = 0.133\delta$ and using the modified Thwaites method to solve for the laminar boundary layer thickness (Thwaites, 1949, Rott and Crabtree, 1952), we find that

$$\frac{\delta_2}{r_H} \approx 0.68\left(\frac{\nu}{r_H U}\right)^{1/2} \tag{11}$$

Then, to account for the decrease in volume flow rate due to the boundary layer, the expressions (6), (7), and (9) should include values for $f_1(y)$ different from unity, namely

$$f_1(y) = \begin{cases} 2\left(\frac{y}{\delta}\right) - 2\left(\frac{y}{\delta}\right)^3 + \left(\frac{y}{\delta}\right)^4 & \text{for } y < \delta \\ 1 & \text{for } y > \delta \end{cases} \tag{12}$$

with $\delta = 5.10(\nu r_H/U)^{1/2}$.

It is also true that the boundary layer will affect the shape of the isobars and therefore cause some alteration of the expressions (3), (5), and (8); we have not included this effect in the present analysis.

3.2 Bubble Screening Effects. In their study of the potential cavitation of nuclei, Johnson and Hsieh (1966) recognized that the relative motion between a nucleus and the liquid might play an important role in determining the number of nuclei which enter the region in which the pressure is below the vapor pressure. Specifically they recognized that a bubble "screening" effect would occur in which the nuclei are forced away from the body due to the large pressure gradients normal to the streamlines in the vicinity of the stagnation point. This outward displacement would be larger for the larger bubbles. Because one is concerned only with streamlines very close to the stagnation streamline and the body surface and because the streamline curvature and therefore the pressure gradient normal to the streamline is much larger in the vicinity of the stagnation point than anywhere else, we may evaluate this screening effect by focusing attention on the stagnation point flow alone. In order to obtain an estimate of this effect we shall assume that the nuclei under consideration (of radius R) are all sufficiently small that the Reynolds number of the relative motion is much smaller than unity. Then the velocity, v, of the nucleus in a direction normal to the streamline is given by

$$v = \frac{2}{9}\frac{R^2}{\mu}\left(\frac{\partial p}{\partial n}\right) \tag{13}$$

where $\partial p/\partial n$ is the local pressure gradient normal to the streamline. Then the total displacement, ϵ, across the streamlines is given by

$$\epsilon = \int_A^B v dt = \int_A^B \frac{v}{|q|}\, ds \tag{14}$$

where $|q|$ is the magnitude of the fluid velocity, the coordinate s is measured along a streamline, A is a point far upstream and B is a location after the large pressure gradients in the vicinity of the stagnation point have been experienced. Note that ϵ will, of course, differ from streamline to streamline and will therefore be a function of r defined as the radial position of the streamline far upstream of the body (see Fig. 5). Thus

$$\frac{\epsilon(r/r_H)}{r_H} = \frac{2R^2U}{9\nu r_H}\int_A^B \frac{1}{\rho U^2}\frac{\partial p}{\partial(n/r_H)}\frac{U}{|q|}\, d\left(\frac{s}{r_H}\right)$$

$$= \frac{2R^2U}{9\nu r_H}\Sigma(r/r_H) \tag{15}$$

where $\Sigma(r/r_H)$ is used to denote the dimensionless integral on the previous line.

Since the stagnation point flow is the same on any blunt axisymmetric body it is appropriate to choose to examine the stagnation region in the potential flow around a sphere in order to evaluate $\Sigma(r/r_H)$. This is a non-trivial calculation, and the details will be omitted here for the sake of brevity. The result is the function $\Sigma(r/r_H)$ presented in Fig. 6; for convenience this can be approximated by the empirical relation

$$\Sigma(r/r_H) = \Gamma(r/r_H)^\gamma \tag{16}$$

where $\Gamma \approx 1.69$, $\gamma \approx 0.5$.

Having evaluated the screening displacement it can be applied to the evaluation of the event rate in the following way. A nucleus of radius R which is on the streamline at radius r far upstream will, when it reaches the low pressure region, be on the streamline which is the following distance, y, from the body surface:

$$\frac{y}{r_H} = \frac{1}{2(1 - C_{PMS})^{1/2}}\frac{r^2}{r_S r_H} + \frac{2}{9}\left(\frac{R}{r_H}\right)^2\frac{r_H U}{\nu}\Sigma(r/r_H) \tag{17}$$

Thus the stream tube between y and $y + dy$ will contain all the nuclei of radius R which were present in the upstream flow between radii r and $r + dr$ (Fig. 5) where

$$\frac{dy}{r_H} = \frac{rdr}{(1 - C_{PMS})^{1/2} r_S r_H} f_2(R, y) \tag{18}$$

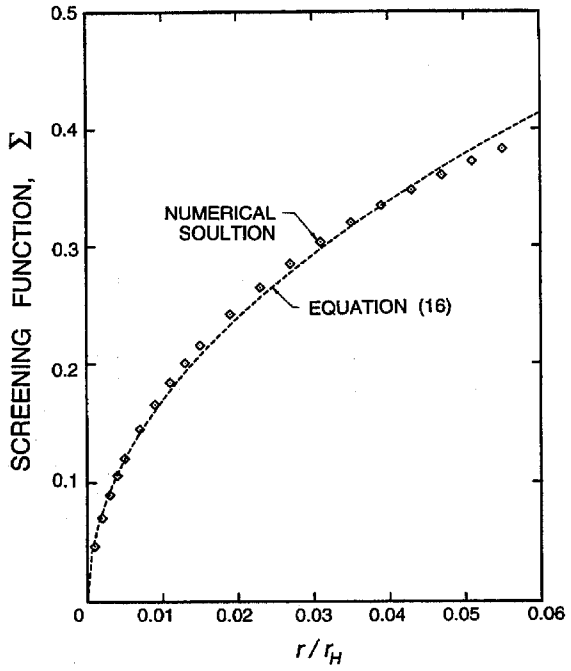

Fig. 6 The function $\Sigma(r/r_H)$ for the stagnation point flow in the potential flow around a sphere

and

$$f_2(R,y) = 1 + \frac{2}{9}\left(\frac{R}{r_H}\right)^2\left(\frac{r_H U}{\nu}\right)(1 - C_{PMS})^{1/2}\left(\frac{r_S}{r_H}\right)\frac{r_H}{r}\Sigma' \quad (19)$$

where Σ' denotes $d\Sigma/d(r/r_H)$ and r and y are related by Eq. (17). Since the liquid flow between y and $y + dy$ is still given by the expression (6), it follows that the actual nuclei number distribution function for the stream tube between y and $y + dy$ is $N_E(R, y)$ where

$$N_E(R, y) = N(R)/f_2(R, y) \quad (20)$$

Consequently, the screening effect alters the event rate by introducing a value for $f_2(R, y)$ different from unity in the expression (9), namely that given by Eq. (19).

3.3 Observable Cavitation Bubble Size Effect. Normally, experimental observation can only detect cavitating bubbles when they achieve a certain observable size, say R_M, and in this section we shall incorporate this "observable cavitation bubble size effect" in our analysis. This requires an analysis of the maximum size, $R_{\max}$, achieved by the cavitation bubble. To do so we approximate the pressure coefficient near the minimum pressure point by

$$C_P = C_{PMS} + \frac{2y(1 - C_{PMS})}{r_K} + \frac{C^*_{P1}|s - s_0|}{r_H}$$

$$= C_{PM} + \frac{C^*_{P1}|s - s_0|}{r_H} \quad (21)$$

where s is a coordinate measured along a streamline and $s = s_0$ is the minimum pressure location and C_{PM} is given by Eq. (3). The value of the constant C^*_{P1} is about 1.39. It follows that the time of residence of the bubble in the region $-C_P \le \sigma$ on a given streamline distance y from the surface is given by

$$t_G = \frac{2(-\sigma - C_{PM})}{UC^*_{P1}(1 - C_{PMS})^{1/2}} r_H \quad (22)$$

The bubble growth rate is given approximately by

$$\frac{dR}{dt} = U(-\sigma - C_{PM})^{1/2} \quad (23)$$

where C_{PM} is given by Eq. (3). It follows that the maximum size reach by a cavitating bubble, $R_{\max}$, will be given roughly by

$$\frac{R_{\max}}{r_H} = \frac{2(-\sigma - C_{PM})^{3/2}}{C^*_{P1}(1 - C_{PMS})^{1/2}} \quad (24)$$

Only those bubbles whose maximum size, $R_{\max}$, is greater than a certain radius, R_M, are regarded as observable cavitation events. By solving $R_{\max} \ge R_M$ for y, we have

$$y \le y_M f_3(R_M/r_H) \quad (25)$$

where

$$f_3\left(\frac{R_M}{r_H}\right) = 1 - \frac{\left[\frac{1}{2}\left(\frac{R_M}{r_H}\right)C^*_{P1}(1 - C_{PMS})^{1/2}\right]^{2/3}}{(-\sigma - C_{PMS})} \quad (26)$$

and y_M is given by (5). Notice that as $R_M \to 0$, $f_3(R_M/r_H) \to 1$. And when

$$\sigma_{cri} = -C_{PMS} - \left[\frac{1}{2}\left(\frac{R_M}{r_H}\right)C^*_{P1}(1 - C_{PMS})^{1/2}\right]^{2/3} \quad (27)$$

$f_3(R_M/r_H) = 0$, which means that if $\sigma \ge \sigma_{cri}$, no bubble with a size greater than R_M will occur. Hence σ_{cri} is the threshold cavitation number. For example, for $C_{PMS} = -0.78$ and $R_M/r_H = 0.04$, σ_{cri} is 0.67, which is significantly less than $-C_{PMS} = 0.78$.

3.4 The Effect of Bubble/Bubble Interactions. As a bubble grows in the low pressure region, the pressure field close to the bubble is altered. Within a certain distance close to the growing bubble the pressure perturbation due to bubble growth increases the local pressure above the critical pressure at which a nuclei will cavitate. Thus, any other nuclei in this volume will not cavitate. In this section we explore this bubble/bubble interaction effect in more detail.

To quantify the effect, we need to calculate the liquid volume in which the local pressure is larger than the Blake (Blake, 1949) critical pressure, p_c,

$$p_c = p_v - \frac{4S}{3}\left[\frac{2S}{3p_{G0}R_0^3}\right]^{1/2} \quad (28)$$

When a bubble is growing, the pressure perturbation in the surrounding liquid is given by

$$\frac{p(r) - p_{\min}}{\rho} \approx \frac{R}{r}(R\ddot{R} + 2(\dot{R})^2) \quad (29)$$

where $p_{\min}$ is the undisturbed liquid pressure. When $R \gg R_0$, the pressure perturbation can be simplified using the Rayleigh-Plesset equation and written as

$$p(r) - p_{\min} = \frac{4}{3}\frac{R}{r}(p_i - p_{\min}) \quad (30)$$

For another nucleus to cavitate, the local pressure must be smaller than the Blake critical pressure. Solving for $p(r) < p_c$, we find the radius of the volume within which another nucleus will not cavitate is:

$$r < \frac{4}{3}\frac{(-C_P - \sigma)}{(-C_P - \sigma - \sigma')} R \tag{31}$$

where σ' is given by

$$\sigma' = \frac{1}{3}\left(\frac{8S}{\rho U^2 R_0}\right)\left[\frac{1}{6}\left(\frac{8S}{\rho U^2 R_0}\right)\frac{1}{\sigma + \left(\frac{8S}{\rho U^2 R_0}\right)}\right]^{1/2} \tag{32}$$

Now, the minimum pressure which a nucleus experiences in flow of the type considered here is a function of the streamline offset, y, normal to the headform surface. And the bubble size at the point where the pressure reaches the minimum pressure is approximately half of the maximum bubble size, $R_{max}/2$. Thus the critical radius is given by

$$r_e = \frac{4}{3}\frac{(-C_{PM}(y) - \sigma)}{(-C_{PM}(y) - \sigma - \sigma')}\left(\frac{R_{max}}{2}\right) \tag{33}$$

and, only those nuclei outside $r = r_e$ can cavitate.

It follows that the number of nuclei which will not cavitate due to the pressure perturbation surrounding a growing bubble is

$$n_i = \int_0^\infty \frac{4}{3}\pi\left[r_e^3 - \left(\frac{R_{max}}{2}\right)^3\right] N(R_0) dR_0 \tag{34}$$

In other words, only one nucleus out of $1 + n_i$ nuclei will actually cavitate. Thus, the effective nuclei number density distribution is given by

$$\frac{N(R)}{1 + n_i} \tag{35}$$

where

$$n_i = \frac{1}{6}\pi R_{max}^3 \int_0^\infty N(R_0) \times \left[\frac{64}{27}\left(\frac{-C_{PM}(y) - \sigma}{-C_{PM}(y) - \sigma - \sigma'}\right)^3 - 1\right] dR_0 \tag{36}$$

Note that the effect of bubble interactions, n_i, is proportional to the cube of the maximum bubble size, R_{max}, which, in turn, is proportional the headform size. This means that, for a small model, bubble interactions may not be very important for the cavitation event rate. But for a large model, interactions may be very important. We do not know that this scaling effect has been recognized before. We also note that when $n_i \gg 1$, it follows that $1 + n_i \approx n_i$, and this implies that, when the bubble interactions become large ($n_i \gg 1$), the event rate becomes independent of the nuclei concentration. This may help to explain the fact that, when the nuclei population is sufficiently large, quantities like the inception number tend to become independent of the nuclei concentration.

4 Results of the Analytical Model

In this section we shall evaluate the various effects on the cavitation event rate and compare the results of the analytical model with the measured cavitation event rates. For this purpose we select a particular nuclei number distribution of the form given by Eq. (1), namely,

$$C = 100 \text{ cm}^{-3}$$
$$\xi = 9.8\ \mu\text{m}$$
$$\lambda = 0.49 \tag{37}$$

These values produce a nuclei distribution which is similar in shape to that of many of the nuclei number distributions which have been measured in the Low Turbulence Water Tunnel and the High Speed Water Tunnel. We note that the concentration, C, of 100 cm^{-3} is also consistent with values obtained by other researchers (see, for example, Billet, 1985). When viewing the analytical results in Fig. 7, one should remember that the cavitation event rates scale almost linearly with concentration C and therefore the results for other values of concentration C are easily obtained. Furthermore, we shall use a minimum observable radius, R_M, of 1 mm since this is the limit of the electrode instrumentation used to detect the cavitation events (see also Ceccio and Brennen, 1992).

First, we present in Fig. 7 typical results calculated for a 5.08 cm Schiebe body at a tunnel speed of 9 m/s. The event rates are calculated from Eq. (9) using the assumed nuclei concentration and distribution (Eqs. (1) and (37)). The individual changes in the event rate due to four separate effects described in Sections 3.1 to 3.4 are shown in the figure, namely the boundary layer flux effect (f_1), the bubble screening effect (f_2), the observable bubble size effect (f_3) and the bubble/bubble interaction effect (n_i). Note that all these effects can produce significant alterations in the event rate, and, together, can account for more than an order of magnitude reduction in the event rate in the present calculation. Among all the effects, the bubble screening effect causes the largest reduction in the event rate. At large cavitation numbers, the effect of bubble/bubble interactions causes little or no reduction in the cavitation event rate. However, at low cavitation numbers, it causes significant reduction because the interactions between bubbles are more intensive at low cavitation numbers due to the larger and more numerous bubbles. The boundary layer flow rate effect is more pronounced at large cavitation numbers since the boundary layer thickness approaches the thickness of the low pressure region in which nuclei cavitate. Also note that the observable cavitation bubble size effect generates a sharp threshold at a cavitation number of about 0.6.

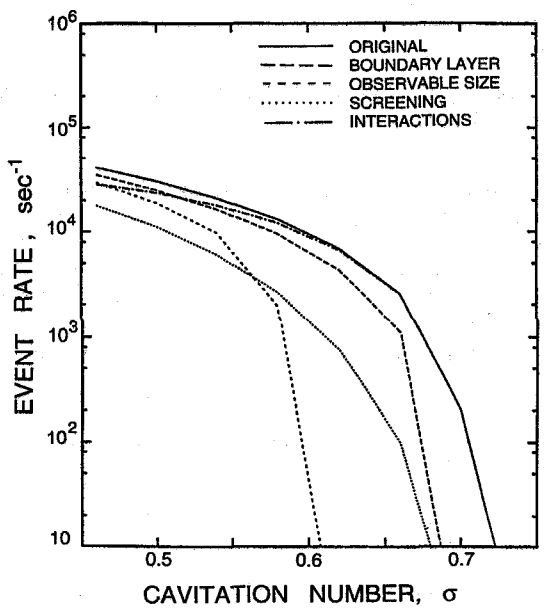

Fig. 7 Typical event rates calculated using an assumed but typical nuclei distribution for flow around a 5.08 cm Schiebe body at a velocity of 9 m/s. Original: Basic method not including the additional effects included in other lines. Boundary layer: As original but including the boundary layer flux effect. Observable size: As original but including only "observable" bubbles larger than 1 mm in radius. Screening: As original but including the bubble screening effect. Interactions: As original but including the bubble/bubble interaction effect.

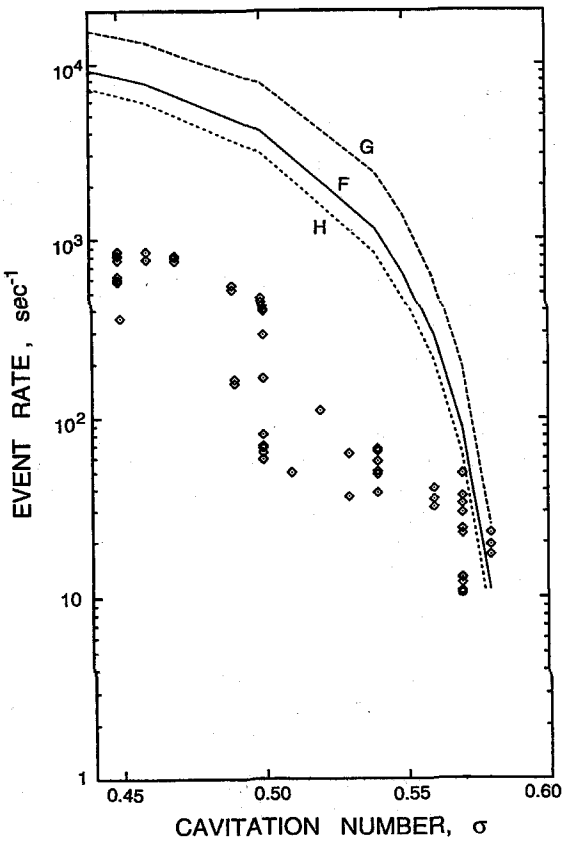

Fig. 8 Left: A comparison of observed cavitation event rates (◇) on a 5.08 cm Schiebe body in the LTWT at a speed of 9 m/sec with anticipated event rates based on simultaneously measured nuclei distributions. The numerical results are plotted as (F): event rates calculated using intermediate nuclei concentrations, (G): event rates calculated using the largest nuclei concentrations, (H): event rates calculated using the smallest nuclei concentrations.

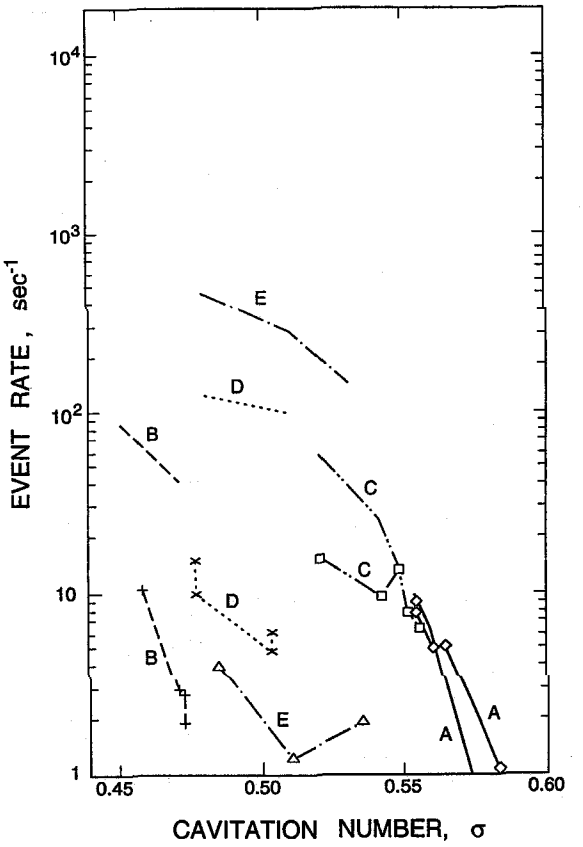

Fig. 8 Right: A comparison of observed cavitation event rates (lines with symbols) on a 5.08 cm Schiebe body in the HSWT reproduced from Fig. 3 with the anticipated event rates (corresponding lines without symbol) based on simultaneously measured nuclei distributions. The uncertainty in the ordinate is ±5 percent.

The effects of the boundary layer flow rate and of bubble screening varied slightly with flow velocity and headform scale. The effects of bubble/bubble interactions, however, varied significantly with headform size since the bubble size increases as the headform size increases. As the headform size increases, the reduction of the cavitation event rate at low cavitation numbers due to bubble/bubble interactions increases with the cube of the headform radius. For the values chosen and at a cavitation number of $\sigma = 0.46$ the bubble interaction factor, n_i, is 0.9 for a headform radius of 2.5 cm. At the same cavitation number, but with a headform radius of 25 cm, the bubble/bubble interaction factor, n_i, is 900, which implies significant reduction in the cavitation event rate. Note, however, in practice that the cavitation on the headform transitioned to fully-attached cavitation long before bubble/bubble interactions reach that level.

Figure 8 presents a comparison between the experimentally measured event rates and the event rates calculated from the analytical model by using the simultaneously measured nuclei distributions. Note that the event rates are in rough agreement at the larger cavitation numbers but that a progressively increasing discrepancy develops as the cavitation number decreases and the event rate increases. At the present time the reason for this discrepancy is not known Though we make several suggestions in the next section.

The information on event rates can be used to produce cavitation inception numbers simply by selecting a certain event rate criterion for inception. In figure 9 we make a qualitative comparison between the inception numbers observed in the LCC experiments of Kuhn de Chizelle et al. (1992) and those calculated from the model using an assumed but typical nuclei distribution function. Both the observed and calculated σ_i are based on an arbitrarily chosen critical event rate of 50 events per second. Comparing the predicted and measured cavitation inception numbers, we note that the trends with changing headform size are consistent. Moreover, the predicted values are also close to those observed experimentally. But the change of the predicted inception numbers with velocity are the reverse of the experiment observations. This is a reflection of the same unresolved velocity scaling issue discussed at the end of Section 2.

We must conclude that two outstanding issues still remain. First the observed event rates at low cavitation numbers are at least one order of magnitude smaller than one would predict based on the anticipated nuclei distributions. Perhaps only a small fraction of the "potential" nuclei actually do cavitate but more detailed study is needed to confirm this. Secondly the changes with tunnel velocity cannot be explained at present. One suspects that the observed effects may be the result of changes in the nuclei population with changes in the tunnel operating condition (pressure and velocity). On-line monitoring of nuclei content and explorations of how the nuclei content changes with operating condition seem essential prerequisites for answering the questions posed by this study. Moreover, it seems clear that cavitation inception criteria are a natural consequence of the event rate variations and that the above recommendations are also an essential prerequisite to an understanding of inception and the scaling effects of cavitation.

5 Conclusions

The present paper describes investigations of the relationship between the cavitation nuclei distributions in the incident free

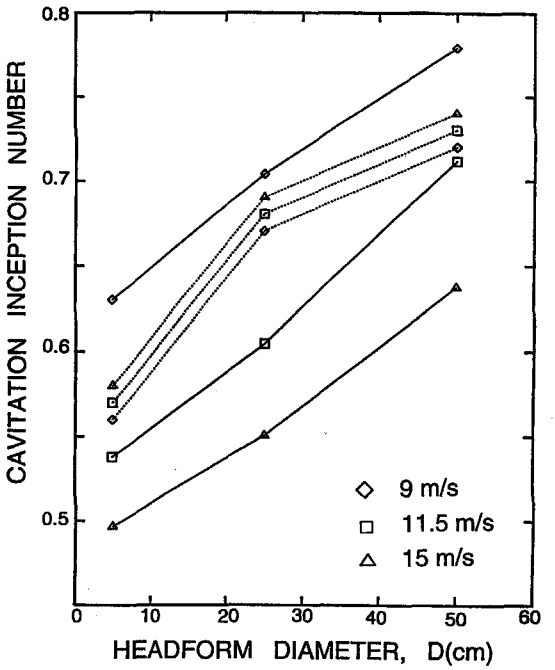

Fig. 9 A comparison of cavitation inception numbers observed in the scaling experiments of Kuhn de Chizelle et al. (1992) (dotted lines) and those predicted by the analytical model based on a critical event rate of 50 s^{-1}, an assumed but typical nuclei distribution and a minimum observable bubble radius of 1 mm (solid lines). Data are shown for three different speeds.

stream and the cavitation event rates on an axisymmetric headform. The cavitation event rates and the nuclei populations in two water tunnels were simultaneously measured. The event rates increase with increasing nuclei population and decreasing cavitation number as expected. However they decrease with increasing tunnel speed even when the nuclei concentrations are similar. This is the inverse of what would be expected.

A simple analytical model is presented for the connection between the nuclei distribution and the event rate. The changes in the cavitation event rate due to several complicating factors are explored; these factors are the reduction of volume flow rate by the boundary layer, the bubble screening effect near the stagnation point, the interactions between bubbles and the effect of a minimum observable cavitation bubble size. Among all these effects, bubble screening results in the largest reduction in the cavitation event rate. However, the effect of bubble/bubble interactions becomes increasingly important with increasing body size and decreasing cavitation number. Combined, all these effects give rise to a reduction in the event rate of an order of magnitude.

The scaling of the predicted cavitation event rate with body size, cavitation number and nuclei population agrees with the experimental observations. At larger cavitation numbers, the predicted cavitation event rates agree quantitatively with the experimental observations in the Low Turbulence Water Tunnel and in the High Speed Water Tunnel. However, two outstanding issues still remain. First the observed event rates at lower cavitation numbers are about an order of magnitude smaller than one would predict based on the actual nuclei distributions. This may be due to the fact that only a fraction of the observed nuclei actually cavitate or it may be due to some other effect not included in the model. One possible effect could be due to the large departure from bubble sphericity; since Kuhn de Chizelle et al. (1995) showed increasing departure from sphericity at low cavitation numbers, this might contribute to the larger discrepancies under those conditions. Other factors might be the increased importance of bubble/bubble interactions at lower cavitation numbers. The other issue which remains is that the changes with tunnel velocity cannot be fully explained at present.

With regard to the possibility that only a fraction of the counted nuclei actually cavitate, we should note that there is some uncertainty regarding the role played by solid particles in the present experiments. Though, in theory, the PDA system should measure only spherical bubbles, in fact, due to the validation level settings some solid particles may also be counted. These may or may not act as nuclei. On the other hand, the validation process may eliminate some bubbles. These uncertainties are, to some extent, resolved by the calibration using the holographic measurements, though that calibration was only possible for nuclei larger than 18 μm. Therefore some of the discrepancies could be caused by the uncertainties associated with solid particles.

When the model for the event rates is used along with some chosen criterion in order to predict the cavitation inception number, the results are consistent with those observed experimentally in so far as the trend with headform size is concerned. The trend with velocity is, of course, at odds with the experiments because of the discrepancy in the event rate discussed above.

Acknowledgments

The authors would like to thank Dr. Yan Kuhn de Chizelle, Dr. Kotaro Sato, Pavel Svitek, Fabrizio D'Auria, Garrett Reisman, Yi-chun Wang, and Elizabeth McKenney for help with the experiments, and Professor Allan Acosta for his advice. This work was supported by the Office of Naval Research under contract number N-00014-91-K-1295.

References

Arndt, R. E. A., and Keller, A. P., 1976, "Free Gas Content Effects on Cavitation Inception and Noise in a Free Shear Flow," *Proceedings, IAHR Conference on Two Phase Flow and Cavitation in Power Generation Systems,* Grenoble, France, pp. 3–16.

Billet, M. L., 1985, "Cavitation Nuclei Measurement—A Review," *Proceedings, ASME Cavitation and Multiphase Flow Forum,* pp. 31–38.

Blake, W. K., 1949, "The Onset of Cavitation in Liquids: I," Technical Report, Acoustics Research Laboratory, Harvard University, Tech. Memo. No. 12.

Cartmill, J. W., and Su, M. Y., 1993, "Bubble Size Distribution Under Saltwater and Freshwater Breaking Waves," *Journal of Dynamics of Atmospheres and Oceans,* Vol. 20, pp. 25–31.

Ceccio, S. L., and Brennen, C. E., 1992, "Observations of the Dynamics and Acoustics of Traveling Bubble Cavitation," *Journal of Fluid Mechanics,* Vol. 233, pp. 633–660.

Feldberg, L. A., and Shlemenson, K. T., 1971, "The Holographic Study of Cavitation Nuclei," *Proceedings, IUTAM Symposium on Non-Steady Flow of Water at High Speed,* Leningrad, USSR, pp. 239–42.

Flynn, H. G., 1964, *Physics of Acoustic Cavitation in Liquids,* Academic Press.

Gates, E. M., and Acosta, A. J., 1978, "Some Effects of Several Free-Stream Factors on Cavitation Inception on Axisymmetric Bodies," *Proceedings, 12th Symposium on Naval Hydrodynamics,* pp. 86–108.

Gates, E. M., and Bacon, J., 1978, "A Note on the Determination of Cavitation Nuclei Distributions by Holography," *Journal of Ship Research,* Vol. 22(1), pp. 29–31.

Gindroz, B., and Billet, M. L., 1994, "Nuclei and Propeller Cavitation Inception," *Proceedings, Cavitation and Gas-Liquid Flow in Fluid Machinery and Devices,* ASME, FED, Vol. 190, pp. 251–260.

Johnson, V. E. and Hsieh, T., 1966, "The Influence of the Trajectories of Gas Nuclei on Cavitation Inception," *Proceedings, 6th Symposium on Naval Hydrodynamics,* Washington D.C., pp. 163–182.

Keller, A. P., 1972, "The Influence of the Cavitation Nucleus Spectrum on Cavitation Inception, Investigated With a Scattered Light Counting Method," ASME *Journal of Basic Engineering,* pp. 917–925.

Keller, A. P., 1974, "Investigations Concerning Scale Effects of the Inception of Cavitation," *Proceedings, Conference on Cavitation,* IMechE, pp. 917–925.

Keller, A. P. and Weitendorf, E. A., 1976, "Influence of Undissolved Air Content on Cavitation Phenomena at the Propeller Blades and on Induced Hull Pressure Amplitudes," *Proceedings, IAHR Symposium on Two Phase Flow and Cavitation in Power Generation System,* Grenoble, France, pp. 65–76.

Kuhn de Chizelle, Y., Ceccio, S. L., and Brennen, C. E., 1995, "Observations, Scaling and Modeling of Traveling Bubble Cavitation," *Journal of Fluid Mechanics,* Vol. 293, pp. 99–126.

Kuhn de Chizelle, Y., Ceccio, S. L., Brennen, C. E., and Shen, Y., 1992, "Cavitation Scaling Experiments with Headforms: Bubble Dynamics," *Proceedings, 19th Symposium on Naval Hydrodynamics,* Seoul, Korea.

Kuiper, G., 1978, "Scale Effects on Propeller Cavitation Inception," *Proceedings, 12th Symposium on Naval Hydrodynamics*, Washington DC, pp. 400–429.

Li, C. Y., and Ceccio, S. L., 1994, "Observations of the Interactions of Cavitation Bubbles with Attached Cavities," *Proceedings, Cavitation and Gas-Liquid Flow in Fluid Machinery and Devices,* ASME. FED, Vol. 190, pp. 283–290.

Liu, Z., 1995, "Nuclei Population Dynamics and Cavitation," Ph.D. thesis, California Inst. of Technology, Pasadena.

Liu, Z., and Brennen, C. E., 1995, "Models of Cavitation Event Rates," *Proceedings, CAV95 International Symposium on Cavitation,* Deauville, France, pp. 321–328.

Liu, Z., and Brennen, C. E., 1994, "The Relation Between the Nuclei Population and the Cavitation Event Rate for Cavitation on a Schiebe Body," *Proceedings, ASME Symposium on Cavitation and Gas Liquid Flows in Fluid Machinery,* pp. 261–266.

Liu, Z., Kuhn de Chizelle, Y., and Brennen, C. E., 1993, "Cavitation Event Rate and Nuclei Distributions," *Proceedings, ASME 4th International Symposium on Cavitation Inception,* New Orleans.

Liu, Z., Sato, K., and Brennen, C. E., 1994, "Cavitation Nuclei Population Dynamics in a Water Tunnel," *Proceedings, ASME Cavitation and Multiphase Flow Forum,* Washington D.C..

Meyer, R. S., Billet, M. L., and Holl, J. W., 1989, "Free Stream Nuclei and Cavitation," *Proceedings, International ASME Symposium on Cavitation Inception,* pp. 55–62.

Meyer, R. S., Billet, M. L., and Holl, J. W., 1992, "Free Stream Nuclei and Traveling Bubble Cavitation," ASME JOURNAL OF FLUIDS ENGINEERING, Vol. 114, pp. 672–679.

Peterson, F. B., 1972, "Hydrodynamic Cavitation and Some Considerations of the Influence of Free Gas Content," *Proceedings, 9th Symposium on Naval Hydrodynamics,* Vol. 2, Paris, France, pp. 1131–1186.

Peterson, F. B., Danel, F., Keller, A., and Lecoffe, Y., 1975, "Determination of Bubble and Particulate Spectra and Number Density in a Water Tunnel with Three Optical Techniques," *Proceedings, 14th International Towing Tank Conference,* Ottawa, Canada, Vol. 2, pp. 27–52.

Rott, N., and Crabtree, L. F., 1952, "Simplified Laminar Boundary Layer Calculations for Bodies of Revolution and for Yawed Wings," *Journal of Aeronautical Sciences,* Vol. 19, pp. 553–565.

Saffman, M., and Buchhave, P., 1984, "Simultaneously Measurement of Size, Concentration and Velocity of Spherical Particles by a laser Doppler Method," *Proceedings, 2nd International Symposium on Applications of Laser Anemometry to Fluid Mechanics,* Lisbon.

Schiebe, F. R., 1972, "Measurement of the Cavitation Susceptibility of Water Using Standard Bodies," Technical report, St. Anthony Falls Hydraulic Laboratory, University of Minnesota, Report No. 118.

Tanger, H., and Weitendorf, E. A., 1992, "Applicability Tests for the Phase Doppler Anemometer for Cavitation Nuclei Measurements," ASME JOURNAL OF FLUIDS ENGINEERING, Vol. 114(3), pp. 443–449.

Thwaites, B., 1949, "Approximate Calculations of the Laminar Boundary Layer," *Aeronautics Quarterly,* Vol. 1, pp. 245–280.